Molecular Recognition of PPARγ by Kinase Cdk5/p25: Insights from a Combination of Protein–Protein Docking and Adaptive Biasing Force Simulations

ARTICLE *in* THE JOURNAL OF PHYSICAL CHEMISTRY B · JUNE 2015

Impact Factor: 3.3 · DOI: 10.1021/acs.jpcb.5b04269 · Source: PubMed

3 AUTHORS:

Melina Mottin

University of Campinas

4 PUBLICATIONS **54** CITATIONS

SEE PROFILE

Paulo Cesar Telles de Souza

University of Campinas

10 PUBLICATIONS **132** CITATIONS

SEE PROFILE

Munir S Skaf

University of Campinas

85 PUBLICATIONS **1,732** CITATIONS

SEE PROFILE

THE JOURNAL OF PHYSICAL CHEMISTRY B

Article

Molecular Recognition of PPAR# by the Kinase Cdk5/p25: Insights from a Combination of Protein-Protein Docking and Adaptive Biasing Force Simulations

Melina Mottin, Paulo C. T. Souza, and Munir S. Skaf

J. Phys. Chem. B, **Just Accepted Manuscript** • DOI: 10.1021/acs.jpcb.5b04269 • Publication Date (Web): 05 Jun 2015

The Journal of Physical Chemistry B is published by the American Chemical Society.
1155 Sixteenth Street N.W., Washington, DC 20036

Molecular Recognition of PPARγ by the Kinase Cdk5/p25: Insights from a Combination of Protein-Protein Docking and Adaptive Biasing Force Simulations

Melina Mottin, Paulo C. T. Souza, Munir S. Skaf*

Institute of Chemistry, University of Campinas-UNICAMP
P.O. Box 6154, Campinas, SP, 13082-864, Brazil

Abstract

The peroxisome proliferator-activated receptor γ (PPARγ) is an important transcription factor that plays a major role in the regulation of glucose and lipid metabolisms and has, therefore, many implications in modern-life metabolic disorders such as diabetes, obesity, and cardiovascular diseases. Phosphorylation of PPARγ by the cyclin-dependent kinase 5 (Cdk5) has been recently proved to promote obesity and loss of insulin sensitivity. The inhibition of this reaction is currently being pursued to develop PPARγ ligands for type 2 diabetes treatments. The knowledge of the protein-protein interactions between Cdk5/p25 and PPARγ can be an important asset for better understanding of the molecular basis of the Cdk5-meditated phosphorylation of PPARγ and its inhibition. By means of a computational approach that combines protein-protein docking and adaptive biasing force molecular dynamics simulations, we obtained PPARγ-Cdk5/p25 structural models that are consistent with the mechanism of the enzymatic reaction and with overall structural features of the full length PPARγ-RXRα heterodimer bound to DNA. In addition to the active site, our model shows that the interacting regions between the two proteins should involve two distal docking sites, comprised of the PPARγ Ω-loop and Cdk5 N-terminal lobe and the PPARγ β-sheet and Cdk5 C-terminal lobe. These sites are related to PPARγ transactivation and directly interact with PPARγ ligands. Our results suggest that β-sheets and Ω-loop stabilization promoted by PPARγ agonists could be important to inhibit Cdk5-mediated phosphorylation.

Keywords: Cdk5, PPARγ, kinase, nuclear receptor, protein-protein docking, molecular dynamics simulations, adaptive biasing force

***Corresponding author**. E-mail: skaf@iqm.unicamp.br

INTRODUCTION

The peroxisome proliferator-activated receptor γ (PPARγ) is an important member of the nuclear receptor (NR) superfamily, which directly binds to DNA and regulates the expression of a myriad of genes related to adipogenesis and control of several cellular signaling, including regulation of insulin sensitization. Pathogenically, PPARγ is involved in the treatment of type 2 diabetes, cardiovascular disease, inflammation, and cancer.[1,2] PPARγ is also a phosphoprotein regulated by phosphorylation additionally to ligand-dependent activation.[3,4] Until now, two phosphorylation sites have been identified in different domains of human PPARγ (subtype 1 sequence numeration): i) S84, located in the N-terminal domain; ii) S245, located within a loop in the ligand binding domain (LBD). The S84 target is phosphorylated by three kinases, the mitogen-activated protein kinases (MAPKs) and the cyclin dependent kinases Cdk7 and Cdk9. Phosphorylation of this site can result in different modulation of PPARγ depending on the kinase involved. The MAPKs repress PPARγ activity through inhibition of the ligand binding and alteration of the cofactor recruitment,[3,4] whereas the reaction promoted by Cdk7 and Cdk9 increases PPARγ activity.[4] The second phosphorylation site, S245 (Fig. 1A), is targeted by Cdk5 which mediates the transfer of a phosphate group from ATP to PPARγ S245 with the assistance of its D126 residue.[5,6] However, the molecular basis of PPARγ activation via phosphorylation by Cdk5 are not yet fully understood.

Cdk5 belongs to a class of enzymes, the cyclin-dependent kinase (Cdk) family. Cdks are proline-directed enzymes, which phosphorylate serine or threonine residues immediately located after a proline.[7,8] Cdk5 is atypical, since unlike other Cdks, it is not directly involved in cell-cycle regulation. Cdk5 plays a role in neuronal development and is pathogenically associated to various neurodegenerative diseases, including Alzheimer's disease and amyotrophic lateral sclerosis.[9,10] Moreover, Cdk5 is not regulated by cyclin activators or autophosphorylation. Instead, Cdk5 is regulated by a different activator known as p25, which is a truncated form of the unstable coactivator

p35.[10,11] The association between the p25 subunit and Cdk5 in the cellular nucleus hyperactivates this kinase enzyme.[12]

Recent studies have shown that Cdk5/p25 also plays a role in pancreatic tissue, being associated with type 2 diabetes. To date, more than 20 proteins with diverse functions have been identified as Cdk5 substrates.[9,10,13,14] Cdk5 is activated in high fat diet obesity induced mice, resulting in PPARγ S245 phosphorylation and, consequently, in dysregulated expression of a subset of obesity related genes without altering PPARγ's adipogenic capacity.[5] Recently, PPARγ partial agonists have been shown to inhibit S245 phosphorylation independently of the classical transcription agonism, which is linked to deleterious side effects.[5] Choi *et al.* reported compounds that have only one binding mode to PPARγ, blocking Cdk5/p25-mediated phosphorylation via non-classical agonist mechanisms, which are still little understood. These specific PPARγ ligands are important antidiabetic targets and further understanding of the structural basis of PPARγ-Cdk5/p25 interactions is highly desirable.

Although Cdk5/p25 crystal structures are available,[7,8,15,16] structures containing a complete substrate associated with Cdk5 (or other Cdks) are lacking. In this work, we use molecular modeling techniques based on protein-protein docking and molecular dynamics (MD) simulations to obtain a model for the PPARγ-Cdk5/p25 complex and study the molecular interactions between Cdk5 and PPARγ. Our results may help elucidating how PPARγ ligands can inhibit Cdk5-meditated phosphorylation of the S245 residue.

MATERIALS AND METHODS

Protein-protein docking

Protein-protein docking experiments were performed with Cluspro 2.0 server,[17–21] an automated rigid-body docking. Cluspro generates 10^9 docking conformations, performing rotation and translation movements of one protein ("ligand") in relation to the other ("receptor", kept fixed). The docking

conformations were ranked based on their clustering properties. The scoring function includes the attractive and repulsive contributions for the van der Waals interaction energy, electrostatic energy, energy of the desolvation contributions and pairwise interaction potentials.[19] The 1000 most energetically favorable docking conformations are clustered (10 to 30 clusters). For this purpose, the program uses a pairwise RMSD-based clustering method to group the docking conformations and find the largest representative clusters of the complex, as described elsewere.[18-21]

The docked structures used are the crystallographic structures of Cdk5/p25 (PDB ID: 1UNL)[8] and PPARγ (PDB ID: 3T03, 1PRG, 1FM6, we used the LBD and removed the ligand).[22–24] We have chosen these PPARγ structure because there are no significant differences between the apo-PPARγ available in protein data bank[25] and this holo-PPARγ without ligand. We performed a blind docking and a docking specifying the attractive site (S245-D126 and P246-V162). As result, there were 180 models, which were classified according to the three criteria: S245(PPARγ)-D126(Cdk/p25) separation, correct Cdk5 consensus sequence, and steric consistency with the intact PPARγ-RXRα-DNA crystallographic structure.

PPARγ-Cdk5/p25 structures preparation

Although Cluspro performs a van der Waals minimization of the models, the minimized structures were not used in the next steps. The minimized PPARγ structure was substituted by the crystal structure (PDB ID: 3T03) without the ligand.[22] Only structural water molecules closer than 5 Å from any PPARγ residue were considered. Some missing residues in this structure (206-209 and 258-276) were taken from the structure of the 1FM6 (PPARγ-RSG complex).[24]

In lieu of a crystal structure for a substrate-bound Cdk5/p25, we built a Cdk5/p25 structure with the active site in proper position for the phosphorylation reaction. Cdk5 has about 60% sequence

identity with Cdk2. However, if only the active site (residues at 5 Å from ATP and Mg^{2+} ions) is considered, the identity is 100%, which allows us to use the Cdk2 active site as a template for modeling the active site of Cdk5. The Cdk5/p25 (PDB ID: 1UNL)[8] and Cdk2/cyclin A-peptide (PDB ID: 3QHW)[26] structures were employed to build the target structure for the MD simulations. The Cdk5/p25 structure presents an inhibitor molecule and was chosen because is the highest resolution structure available among the others Cdk5 in the protein data bank. The Cdk2/cyclin A-peptide structure is a transition state complex bound to ADP, MgF^{3-} (a mimic for the γ-phosphate of ATP), two Mg^{2+} ions and substrate peptide. The coordinates of this structure used to model the active site of Cdk5 are: D126, ADP, MgF^{3-}, Mg^{2+} ions, water molecules close to Mg^{2+} ions (important for the Mg^{2+} hexacoordination) and the PKTPK sequence of the peptide. The ATP molecule has been based on the position of the ADP and MgF^{3-}. We took only 5 residues of the peptide sequence that was mutated to DKSPF, as the PPARγ sequence. For both proteins, PPARγ and Cdk5/p25, hydrogen atoms were added and the protonation states of the histidine residues were estimated with H++ server[27] at pH 7.4. The positions of the hydrogen atoms, in neutral histidines, were defined in such a way to favor hydrogen bonds.

The entire system as solvated by a water shell of at least 15 Å from the protein surface and neutralized in a NaCl concentration of 0.15 mol/L using the VMD[28] plugins solvate and autoionize, respectively. Then we performed an energy minimization and equilibration. All simulations were carried out using NAMD2.9[29] with CHARMM22/CMAP[30,31] force field for the protein and the TIP3P model for water molecules.[32] We performed 1000 steps of energy minimization to remove side chain bad contacts and 5 ns of pre-equilibration MD to relax the structure, maintaining the bonds and angles of the active site fixed. This procedure was performed to relax only the region around the active site, which was adapted from Cdk2.

Adaptive Biasing Force (ABF) MD simulations[33–35] were carried after aligning and replacing the PPARγ-Cdk5/p25 initial candidates obtained from Cluspro docking by the structures prepared as

described above. The PPARγ-Cdk5/p25 models were than solvated and electro-neutralized by addition of Na^+ and Cl^- ions at 0.15 mol/L. The final model systems contained approximately 120,000 atoms.

Refinement of the PPARγ-Cdk5/p25 models

ABF MD techniques[33–35] were used to approximate the phosphorylation residues at a sufficient distance capable of promoting the reaction (Fig. 2). The RMSD values of the phosphorylation site residues were used as colletive reaction coordinates to represent the approximation process . The reference structure for calculating the RMSDs was based in the catalytic residues of the Cdk5/p25-peptide modeled structure (position of the S245 in the peptide substrate, D126, N131, D144, V162 residues, ATP and two Mg^{2+} ions). The RMSD reaction coordinate has a range of allowed values from 3.5 Å (initial PPARγ-Cdk5/p25 model obtained with Cluspro) to 0 Å (refined model), with a force constant of 10 kcal/mol/$Å^2$ as boundary potentials. In order to obtain a smooth relaxation, a threshold of 1,000,000 force samples sufficed to obtain a reasonable estimate of the force distribution, and, hence, of the average force, which were subsequently applied along the reaction coordinate.

Approximately 110 ns of ABF MD simulations were performed until the (H)S245-(O)D126 distance stabilized around 2Å. The simulations were performed using periodic boundary conditions in the NpT ensemble at temperature of 298 K and pressure of 1 atm. Langevin thermostat and Langevin/Nosé-Hoover piston barostats were used for the temperature and pressure control, respectively. Electrostatics were evaluated using the Particle Mesh Ewald[36] algorithm and short-range interactions were truncated at a cutoff radius of 12 Å. All bonds involving apolar hydrogens were constrained at their equilibrium values using the algorithm SHAKE[37] and a timestep of 2.0 fs was used for the integration of the equations of motion.

The following treatment was used to prepare the systems for the production runs: (A) 1000 energy minimization steps using the conjugate gradients algorithm (CG) followed by 400 ps of MD

keeping protein, ATP and Mg^{+2} ions fixed; (B) 2000 energy minimization steps using CG followed by 1 ns of MD keeping all protein except residues less than 8 Å of ATP and Mg^{+2} ions and the modeled residues fixed; (C) 2000 energy minimization steps using CG followed by 2 ns of MD keeping all backbone protein except residues less than 8 Å of ATP and Mg^{+2} ions and the modeled residues fixed. After these preparation steps, ABF MD trajectories of 110 ns for each model were generated. The final structures of these simulations are evaluated by PROCHECK.[38,39] The stereochemical quality of the structures showed that, on average, 92% of residues remained in most favored regions (representing the most favorable combinations of phi-psi values). For a good quality model, over 90% of the residues should be in this core region.

Molecular Dynamics of the PPARγ-Cdk5/p25 models

The starting structures for the conventional MD simulations of the PPARγ-Cdk5/p25 models were arbitrarily taken from the ABF MD runs, for which the (H)S245-(O)D126 distance was less than 2.5 Å and the average RMSD of the S245 loop (PPARγ) was smaller than 2Å. We performed 300 ns of conventional MD for each model. In the first 10 ns of simulation, we added an extra harmonic bond between (H) S245 – (O) D126 bond and also extra harmonic bonds and angles to keep the two Mg^{2+} ions hexacoordinated. The parameters were set to 10 kcal/(mol·Å^2) for the force constant, 2 Å for the reference equilibrium distance, and 90° or 180° for the reference equilibrium angles. After this equilibration time, only the Mg^{2+} ions hexacoordination was maintained fixed. We used the same ensemble, temperature, pressure and electrostatics conditions used in ABF simulations.

Accelerated Molecular Dynamics of free-PPARγ LBD

Accelerated molecular dynamics (aMD)[40–43] simulations were carried out for the crystallographic structure of PPARγ (PDB ID: 3T03), in which the ligand was removed. The

simulations were performed using periodic boundary conditions in the NVT ensemble at temperature of 298 K using the Langevin thermostat for the temperature control. The systems are comprised of approximately 58,000 atoms and fully solvated with a water shell of at least 15 Å. The PPARγ LBD systems for the production aMD runs were prepared as follows: (A) 500 energy minimization steps using the conjugate gradients algorithm (CG) followed by 20 ps of MD keeping all the ligand and protein fixed; (B) 500 energy minimization steps using CG followed by 20 ps of MD keeping only modeled residues fixed (C) 500 energy minimization steps using CG followed by 20 ps of MD keeping only the α carbons fixed. After these preparation steps, aMD trajectories of 200 ns were generated for analysis. The boost parameters were set based upon the average dihedral energy calculated by performing a short classical molecular dynamics (MD) simulation, E = 2128 kcal mol^{-1} e α = 217.6 kcal mol^{-1}, according to the literature.[43]

RESULTS AND DISCUSSION

We have combined different computational techniques to predict structural models for the interaction between Cdk5/p25 and PPARγ. Our approach, schematically represented in Fig. 1, starts with a protein-protein docking of Cdk5/p25 and PPARγ crystal structures (Fig. 1A) to generate a collection of initial structures for the complex. The ensemble is narrowed down to a few selected model candidates (Fig. 1B) by taking into account the biochemistry of the phosphorylation reaction and the crystallographic structure of the full-length PPARγ-RXRα heterodimer complex.[44] The candidate structures were adjusted by means of ABF MD simulations using as target the crystal structure of a Cdk2 enzyme bound to a peptide substrate,[26] as depicted in Fig. 1C. The resulting putative models were subsequently subjected to unconstrained MD simulations (Fig. 1D), from which the structural stability of the models was assessed. Accelerated MD (aMD) simulations of the apo-PPARγ LBD were also carried out to examine the conformational freedom of the S245 loop in the absence of the Cdk5's

influence and compare it to the models.

Docking PPARγ to Cdk5/p25

A set of 180 initial structures of the PPARγ-Cdk5/p25 complex were obtained from the Cluspro protein-protein docking server[18–21] using the crystallographic structures of Cdk5/p25[8] and PPARγ.[22–24] The ligands of holo-PPARγ structures were not considered for predicting the models because their interaction with the LBD may block the action of Cdk5.[5,6] The ensemble of PPARγ-Cdk5/p25 docked poses was reduced to 12 candidates by selecting only model structures in which the PPARγ surface that contains the residue S245 faces the Cdk5/p25 catalytic site. This was obtained by selecting structures in which the distance between the S245 (PPARγ) and D126 (Cdk/p25) residues was less than 15Å. The ensemble was further reduced to 4 candidate structures by selecting poses which satisfied the correct consensus sequence of Cdk5 recognition of substrates (residue sequence X_{-1} S/T_0 P_{+1})[7,16] (Supplemental Fig. 1), and exhibited no substantial steric hindrance between Cdk5 and the intact PPARγ-RXRα-DNA crystal structure (Supplemental Fig. 2).[44]

Although the resulting 4 candidate models are distinguishable from each other, they exhibit similar Cdk5/p25 arrangements relative to PPARγ. To interact with PPARγ and respect Cdk5 consensus sequence, the C-terminal lobe of Cdk5 must be directed to β-sheet region of PPARγ, while the Cdk5 N-terminal lobe and p25 are directed to Ω-loop. The candidate model complexes suggest that the main contact regions between PPARγ and Cdk5/p25 are PPARγ's β-sheet, the S245 loop, helix 2' and the Ω-loop.

Refinement of PPARγ-Cdk5/p25 models

Although the protein-protein docking and selection criteria have allowed identifying some overall features of the candidate model complexes, further structural adjustments are necessary in order

to bring the phosphorylation target region of PPARγ (the loop containing S245) properly positioned in the Cdk5 active site. The ABF MD method,[33–35] which is widely used to enhance conformational sampling and estimate free energy between states,[34] was chosen to refine the 4 candidate models, as schematically represented in Fig. 2A. Starting from the protein-protein docking structures, we performed 110 ns of ABF MD for each model using an available crystal structure for a peptide bound to Cdk2 (a Cdk5 homologous) as reference structure and the RMSD of phosphorylation site residues as reaction coordinate.

During the course of ABF MD runs, generalized forces are smoothly applied to specified residues and drive the reaction coordinate to the target reference structure (Fig. 2B). Key residues at the catalytic site of the reference Cdk2 (blue) and ABF-refined Cdk5 (green) kinases, as well as the peptide (blue) and PPARγ (green) substrate serine residues are shown (Fig. 2B). The two distinct Mg^{2+} ions and the ATP molecule are also shown. The time-history along the ABF MD runs for the RMSD reaction coordinate and the S245-ATP and S245-D126 distances, shown in Fig.2C, indicates that the structures of the 4 PPARγ-Cdk5/p25 candidate models were satisfactorily adapted. The last 10 ns of ABF simulations were used for further structural analysis, since in last part of the trajectory the average distances between H-S245 and O-D126 fluctuates around 3Å (Fig. 2C). The atomic coordinates of PPARγ-Cdk5/p25 models can be obtained from the authors upon request.

Figure 3A shows aligned snapshots of PPARγ from the starting protein-protein docking (grey) and end of ABF simulations (violet). Models 1 and 3 have undergone significant repositioning (translation and rotation of the PPARγ LDB relative to Cdk5/p25) during the ABF refinement process compared to Models 2 and 4. During the ABF MD runs on Models 1 and 3, a substantial Cdk5/p25 approximation toward the PPARγ β-sheet region was observed. Noticeable conformational changes were also observed in the Ω-loop that helped to maintain the interaction between PPARγ and Cdk5/p25. Nevertheless, no significant internal structural changes occurred on PPARγ, Cdk5 or P25

relative to their respective crystal structures during ABF, as indicated by the average RMSD values of their backbone which fluctuate around 2Å for each protein (crystallographic structures as references) (Fig. 3B).

These results show that the ABF-based refinement of the initial PPARγ-Cdk5/p25 docking models reorganized the structural arrangement so that the kinase and the substrate are properly positioned for the phosphorylation reaction, while preserving most of their individual structures.

Because the S245 loop (the phosphorylation target) and the adjacent β-strand are highly mobile parts of the PPARγ LBD, it is important to examine whether the ABF-refined models produced conformations that are compatible with the local structural fluctuations exhibited by the apo-PPARγ LBD in these regions. In order to sample conformational fluctuations of the apo-LBD, we carried out simulations using accelerated molecular dynamics (aMD) techniques, which essentially enhance conformational sampling by raising the basins of the dihedral potential energy surface without affecting the general form of the atomistic potential.

Results from the aMD simulations of apo-PPARg and from the last 10 ns of the ABF MD runs for Models 1-4 were obtained for the average RMSD values of the S245 loop and β-strand (Fig. 4A) and the average fraction of native contacts between the S245 loop and the rest of the PPARγ LBD (Fig. 4B), relative to the crystallographic PPARγ structures. The structural deviations of the S245 loop and β-strand regions in Model 1 relative to the reference crystal structure (~6.4 Å) are considerably higher than that exhibited by the other models and even higher than the ligand-free PPARγ subjected to aMD (~5 Å). Results for the average percentage of contacts between residues in the S245 loop and the rest of PPARγ (Fig. 4B), indicate that in Model 4 the S245 loop maintains a substantial contact with PPARγ (~75%), whereas in Model 1 more that 50% of the contacts are lost, suggesting the S245 loop is detaching from the LBD surface in this model.

Figure 4C shows superimposed structures for the H2/S245 loop/β-strand region extracted from the apo-PPARγ aMD simulations (light grey) and representative snapshots of ABF MD for Models 1-4 (colors). For comparison, the crystal structure is also shown (dark grey). We observe that β-sheet secondary structures were preserved in all models, but conformational changes in the S245 loop are markedly apparent for Model 1. In fact, the S245 loop assumes conformations in Model 1 that were not at all sampled by the aMD simulations on free-PPARγ. Taken together, these results seems to suggest that if the PPARγ-Cdk5/p25 complex structure portrayed by Model 1 would hold true, the process of Cdk5 approximation and binding to PPARγ would involve an induced fit mechanism.[45,46] In this case, the interaction of Cdk5 with PPARγ induces a conformational change in the S245 loop region to subsequently promote the phosphorylation reaction. For the other models, the ABF snapshots indicate that the S245 loop in the complex assumes conformations that are similar to those frequently visited by the apo-form of PPARγ, i.e. conformations that were in preexisting equilibrium dynamics of the apo-PPARγ.[45,47,48]

These results also indicate that, for PPARγ-Cdk5/p25 Models 2-4, substantial changes in the S245 loop conformation are not required for interaction with Cdk5. In these models, the S245 loop adopts conformations similar to the crystal structures of PPARγ bound to agonist ligands, where the loop is in a closed conformation against the body of the LBD. Only Model 1 follows the assumption that S245 loop is unstable in the absence of ligand and detaches from the PPARγ surface for interaction with the Cdk5. This hypothesis is supported by Choi *et al.*, based on the high levels of deuterium incorporation in this region.[5]

Relaxation and Structural Stability of PPARγ-Cdk5/p25 models

To test which docking architecture (and hence which model) best represents the PPARγ–Cdk5/p25 complex is necessary to check their stabilities. For that purpose, we carried out 300 ns

unconstrained MD simulations of each PPARγ-Cdk5/p25 model to relax the complexes and verify the stability of their protein-protein interactions. Figure 5A shows the distance between H-S245 (PPARγ) and O-D126 (Cdk5) at the phosphorylation site during the course of these simulations. In Models 1 (orange) and 2 (navy blue), the loop detached from the phosphorylation site of Cdk5 in the beginning of the simulation (around ~ 10 ns) and the serine residue turns toward the PPARγ LBD (Fig. 5A, 5B, 5C). In Model 1, the S245-D126 contact is replaced by an interaction between S245 and Q345 (residue in the β-sheet region) and in Model 2, by interactions between S245 and neighboring water molecules. At ~125 ns of simulation time, the S245 residue in the Model 4 (green line in Fig.5A; Fig. 5D) also departs from D126; initially S245 interacts with residue K261 of PPARγ and then with water molecules. By contrast, in Model 3 the phosphorylation site residues remained close to each other during the entire course of the simulations (magenta line in Fig.5A). In Figure 5E, we observed the S245 residue was toward to the D126 residue. S245 sometimes interacts with E161 (Cdk5), but remains close to D126 for eventual interaction.

In the light of these results, the ABF-refined Model 3 seems a better candidate to represent PPARγ-Cdk5/p25 interactions. However, we cannot rule out the other models, especially Model 4, because besides the similarity between the proposed model structures, it is not known how long PPARγ-Cdk5/p25 have to be engaged in a complex formation for the phosphorylation reaction to occur. There are, nevertheless, some similarities and differences between Models 3 and 4 (and the other models) that are discussed in the Supplementary Material.

Cdk5/p25-PPAR Model description: three docking regions

In this section, we further analyze Model 3, highlighting the main interactions and conformational changes involved upon association of PPARγ and Cdk5/p25. The molecular characterization of Model 3, after ABF refinement, shows that the PPARγ – Cdk5/p25 interface can be

subdivided into three main contact regions, as shown in Fig.6A: the Ω-loop site, formed by the PPARγ Ω-loop and the Cdk5 N-terminal lobe, the active site, established between the PPARγ S245 loop and the Cdk5 catalytic residues, and the β-sheet site, comprised of the PPARγ β-sheet and the Cdk5 C-terminal lobe. These three contact regions or sites are common to all models obtained here, with some changes in the number and type of interactions (Supplemental Fig. 3). The Ω-loop and the β-sheet sites can be described as examples of distal docking sites, i.e. additional binding motifs spatially separated from the active site of an enzyme. Their function includes increasing the affinity and specificity for the substrates. Therefore, the Ω-loop and the β-sheet sites could increase the local substrate concentration and hence the rate of phosphorylation.[49] Distal docking sites have been identified in various kinases, including Cdk2.[50–52] Located on the cyclin partner about 40 Å away from the active site, this Cdk2 distal docking site involves a hydrophobic region (as observed in PDB ID: 2CCI)[52] that interacts with the RXL motif substrate peptide. The Ω-loop region of PPARγ seems to be in a similar position of the RXL motif, and can involve interactions with p25 partner of Cdk5 as found in Model 3. However, the Ω-loop region is located closer to the active site (about 25 Å) and could involve both hydrophilic and hydrophobic interactions.

Figures 6B-D show in detail the interactions between the residues in active and distal sites. In Ω-loop site (Fig. 6B), K265 (Ω-loop of PPARγ) interacts via a hydrogen bond with E42 (β3-αC loop of Cdk5) and K261 (Ω-loop of PPARγ) establishes a salt bridge with E240 (α3-α4 loop of p25) and E161 (β9-αF loop of Cdk5). The M257 residue, also in Ω-loop of PPARγ, makes a hydrophobic contact with A160 (β9- αF loop of Cdk5). In the active site (Fig. 6C), S245(PPARγ) interacts via hydrogen bonds with D126 (β6-β7 loop of Cdk5) and with the ATP molecule. The other interactions of this site are mainly hydrophobic; the P246 residue, especially, in S245 loop of PPARγ, which makes a hydrophobic cluster with V162 (β9-αF loop of Cdk5) and L147 (β8-β9 loop of Cdk5). The third site is the β-sheet site, formed by only hydrophilic interactions. In this region, K336 (β2-β3 loop in PPARγ) interacts with

D210 of αG in Cdk5 and a saline cluster is formed. The adjacent residue D337 (β2-β3 loop in PPARγ) maintains the position of K336 and the R214 residue in αG in Cdk5 maintains D210 position (not shown in Fig. 6D). Close to these residues lies N335 (β2-β3 loop in PPARγ), which makes a polar interaction with N206 (αF-αG loop) in Cdk5. Residue T349 (β4) in PPARγ forms a hydrogen bond with D207 (αF-αG loop) in Cdk5 and the residue E351 (β4) in PPARγ interacts with K237 (αG-αH loop) in Cdk5. The residues N253 (H2') in PPARγ and D235 (αG-αH loop in Cdk5) interact by via hydrogen bond. To discriminate the amount and the type of interactions in each site we computed the number of hydrophilic and hydrophobic contacts (Fig. 6E).

The complementarities of the described interactions may contribute to the selectivity of Cdk5 by certain substrates in relation to other members of this kinase family. For example, it is reasonable to expect that Cdk2 is not able to phosphorylate PPARγ, since these proteins have completely different cellular functions. In spite of that, the active site and the amino acid substrate specificity of Cdk2 (X_{-1} S/T_0 P_{+1} X_{+2} (K,R_{+3})) are identical to the Cdk5.[52] The primary sequence alignment of Cdk2 and Cdk5 (Supplemental Table 1) indicate that the main differences between residues are located in the Ω-loop and β-sheet sites. In these regions, we find that some residues, in same position of Cdk5 and Cdk2 sequences, differ with respect to their chemical nature, possible reducing the interactions with PPARγ. To illustrate this point, consider a residue in position 160, which in Cdk5 is occupied by an alanine and in Cdk2 corresponds to the basic residue histidine, which certainly causes a penalty for the hypothetical Cdk2-PPARγ association. Moreover, Cdk2 has no hydrophobic residues in this region to compensate the interaction with M257 of PPARγ. These are indications that the distal docking regions of Model 3 may be at least partly responsible for the selectivity of Cdk5 for certain substrates.

The main structural alteration observed in the Model 3 relative to the crystallographic structures, occurs in the Ω-loop region of PPARγ, which detaches from the PPARγ LBD core to preserve PPARγ-Cdk5/p25 contacts. In the active site, the interactions between P246-V162 and S245-

D126, and mainly the orientations of these contacts, are important to substrate recognition by Cdk5. It has been reported that Pro-directed kinases create a nonpolar pocket to accommodate the proline residue.[49] Like in Cdk2, in our refined Model 3 the V162 (Cdk5) makes a hydrophobic contact with P246 (PPARγ) (Fig. 6C). In this region, PPARγ and Cdk5 present other hydrophobic complementary residues, such as V248 (PPARγ), L147 (Cdk5) and L165 (Cdk5). Thus, we advocate that Cdk5 provides an adequate hydrophobic environment to accommodate the PPARγ P246 residue, promoting interactions not only with V162.

The proposed Model 3 suggests all three docking regions could be important to mediate Cdk5 binding to PPARγ. PPARγ β-sheets seem to be a slightly more rigid docking region, which may serve to properly orient the Cdk5 with respect to the S245 phosphorylation site. Meanwhile, PPARγ Ω-loop is an adaptable region and may change its conformation to allow for effective interactions with Cdk5. The Ω-loop flexibility could enable the Cdk5 docking to PPARγ in slightly different ways. Since Cdk5/p25 acts in a wide range of substrates, it is plausible that the enzyme-substrate interactions are able to slightly adapt depending on the substrates.

Insights about PPARγ function and phosphorylation inhibition

An interesting feature of our PPARγ-Cdk5/p25 models is that the β-sheet and Ω-loop interaction sites are reported in the literature as activator regions in PPARγ,[54,55] but have not been linked to phosphorylation. Although the most well-known PPARγ activation mechanism involves conformational alterations in helix H12,[23] other regions in PPARγ LBD are also important for transcriptional activation. Bruning and colleagues have shown that β-sheets and Ω-loop can be mediators of graded transcriptional response of PPARγ,[54] dependent on the degree of ligand agonism. Hydrogen-deuterium exchange (H/DX) experiments comparing full, partial and intermediate agonists of PPARγ have shown that, unlike full agonists, intermediate and partial agonists highly protect the H/D exchange in the β-

sheet region, suggesting a stabilization of the region.[54] Conformational changes in the Ω-loop activates PPARγ via fatty-acids metabolites and mutations in the Ω-loop and in its vicinity completely abolishes this activation route.[55] This region has also been related to activation of other PPARs isotypes[56] and even other NRs, which suggests a possible ligand association/dissociation pathway.[57–59] Other studies recently have shown that a partial agonist reduces the mobility of the β-sheet and S245 loop, putting the latter in a less favorable configuration to Cdk5 attack.[5] In fact, the most recent efforts in search of a PPARγ-related treatment for type 2 diabetes are focused on inhibitors to the Cdk5-medited S245 phosphorylation.

Blocking of the phosphorylation reaction may be achieved by at least two obvious pathways: by impairing the activity of the enzyme itself or via substrate. Cdk5 is a pleiotropic enzyme involved in several cellular processes, including membrane transport, cell adhesion, neuronal migration, actin dynamics, synaptic structure and plasticity and myogenesis.[14] The enzyme blockade is likely to cause serious deleterious consequences in different cell domains. Therefore, a less impactful and possibly more viable alternative would be via ligand-induced conformational changes that may control the relevant PPARγ regions, and hopefully hinder the enzymatic action on this particular substrate.

The main conformational differences in the PPARγ LBD observed between our Model 3 (after ABF refinement) and the crystallographic holo-PPARγ structures with different ligands involve the Ω-loop. Aligned crystal structures of PPARγ-full agonists (PDB ID: 2ATH,[60] 2F4B[61]) and PPARγ-partial agonists (PDB ID: 2I4Z,[62] 3B3K[63]), as well as our PPARγ-Cdk5/p25 Model 3 are shown in Fig.7. In the (Cdk5-free) crystallographic structures of PPARγ, the Ω-loop lies close to the PPARγ LBD core, whereas in our PPARγ-Cdk5/p25 Model 3, the Ω-loop acquires an open configuration. This conformation enables the interaction between PPARγ Ω-loop and Cdk5/p25 and could explain the phosphorylation inhibition promoted by PPARγ ligands. PPARγ ligands can induce conformational changes in the LBD, especially in β-sheet and Ω-loop regions.[5,54,55,64] These modifications may keep

the Ω-loop in a closed configuration, thus preventing the PPARγ-Cdk5/p25 binding mode, as portrayed by our Model 3, and, consequently, may impair S245 phosphorylation.

CONCLUDING REMARKS

We have proposed structural models for the complex formed by the binding of the Cdk5/p25 enzyme to the substrate PPARγ LBD, which were obtained by combining rigid protein-protein docking and molecular dynamics simulation techniques. Initial model candidates were first obtained from docking that satisfied some general features, including proper orientation of the enzyme-substrate interface and consensus sequence, and compatibility with the crystal structure of the full-length intact heterodimer PPARγ-RXRα bound to a DNA stretch, representative of a hormone response element. The initial model candidates obtained from the rigid protein-protein docking, however, failed to reproduce the adequate molecular arrangement for the phosphorylation reaction at the catalytic site. Further adjustments in the model structures were performed by means of ABF MD simulation techniques using the crystal structure of the homologous Cdk2 kinase bound to an oligopeptide as target. Using this approach, we were able to add the necessary flexibility to the side chains and backbone atoms of the proteins to achieve the proper molecular arrangement at the catalytic site for the phosphorylation reaction. Atomistic MD simulations further validated the proposed models and their main characteristics were analyzed. In addition to the active site, two distal regions – PPARγ's Ω-loop and β-sheets – were identified which may play an important role in the interaction of Cdk5 with the nuclear receptor. The implications of these results to the development of PPARγ ligands that promote inhibition S245 phosphorylation by Cdk5 are discussed.

Future studies would be highly desirable in order to experimentally validate the proposed PPARγ-Cdk5/p25 model. These could include, for instance, small-angle X-ray scattering (SAXS) to assess the three-dimensional architecture of the PPARγ-Cdk5/p25 complex (if the complex is sufficiently long-

lived in solution). Chemical cross-linking and mass spectrometry techniques could also be used for this purpose, allowing for the determination of distance restraints between residues at the enzyme-substrate interface.[65,66] Moreover, site-directed mutagenesis assays could be performed to investigate how mutations in β-sheet and Ω-loop regions of the apo-PPARγ structure may affect phosphorylation of the S245 residue.

Associated Content

Supporting Information

Supporting Figures S1-S4 and supporting Table S1, for comparison between the proposed PPARγ-Cdk5/p5 models. Atomic coordinates of the four PPARγ-Cdk5/p25 models are also available in PDB format. This material is available free of charge via the Internet at http://pubs.acs.org .

Author Information

Corresponding Author. E-mail: skaf@iqm.unicamp.br

Acknowledgments

This work was supported by the Sao Paulo Research Foundation FAPESP (2013/08293-7, 2011/22735-7, 2012/24750-6). The authors declare no conflicting interest.

REFERENCES

(1) Lehrke, M.; Lazar, M. A. The many faces of PPARgamma. *Cell* **2005**, *123*, 993–999.

(2) Desvergne, B.; Wahli, W. Peroxisome proliferator-activated receptors : Nuclear control of metabolism. *Endocr. Rev.* **1999**, *20*, 649–688.

(3) Pang, X.; Shu, Y.; Niu, Z.; Zheng, W.; Wu, H.; Lu, Y.; Shen, P. PPARγ1 phosphorylation enhances proliferation and drug resistance in human fibrosarcoma cells. *Exp. Cell Res.* **2014**, *322*, 30–38.

(4) Ahmadian, M.; Suh, J. M.; Hah, N.; Liddle, C.; Atkins, A. R.; Downes, M.; Evans, R. M. PPARγ signaling and metabolism: The good, the bad and the future. *Nat. Med.* **2013**, *19*, 557–566.

(5) Choi, J. H.; Banks, A. S.; Estall, J. L.; Kajimura, S.; Boström, P.; Laznik, D.; Ruas, J. L.; Chalmers, M. J.; Kamenecka, T. M.; Blüher, M., et al. Anti-diabetic drugs inhibit obesity-linked phosphorylation of PPARγ by Cdk5. *Nature* **2010**, *466*, 451–456.

(6) Choi, J. H.; Banks, A. S.; Kamenecka, T. M.; Busby, S. A.; Chalmers, M. J.; Kumar, N.; Kuruvilla, D. S.; Shin, Y.; He, Y.; Bruning, J. B., et al. Antidiabetic actions of a non-agonist PPARγ ligand blocking Cdk5-mediated phosphorylation. *Nature* **2011**, *477*, 477–481.

(7) Tarricone, C.; Dhavan, R.; Peng, J.; Areces, L. B.; Tsai, L.; Musacchio, A. Unit SB. Structure and regulation of the CDK5-p25. *Mol. Cell* **2001**, *8*, 657–669.

(8) Mapelli, M.; Massimiliano, L.; Crovace, C.; Seeliger, M. A.; Tsai, L. H.; Meijer, L.; Musacchio A. Mechanism of CDK5/p25 binding by CDK inhibitors. *J. Med. Chem.* **2005**, *48*, 671–679.

(9) Arif A. Extraneuronal activities and regulatory mechanisms of atypical cyclin dependent kinase Cdk5. *Biochem. Pharmacol.* **2012**, *84*, 985–993.

(10) Ahmed, D.; Sharma, M. Cyclin-Dependent Kinase 5/p35/p39: A Novel and imminent therapeutic target for diabetes mellitus. *Int. J. Endocrinol.* **2011**, *2011*, 1–10.

(11) Patrick, G. N.; Zukerberg, L.; Nikolic, M.; de la Monte, S.; Dikkes, P.; Tsai, L. Conversion of p35 to p25 deregulates Cdk5 activity and promotes neurodegeneration. *Nature* **1999**, *402*, 615–622.

(12) Shukla, V.; Zheng, Y. L.; Mishra, S. K.; Amin, N. D.; Steiner, J.; Grant, P.; Kesavapany, S.; Pant, H. C. A truncated peptide from p35, a Cdk5 activator, prevents Alzheimer's disease phenotypes in model mice. *FASEB J.* **2013**, *27*, 174–186.

(13) Wang, C. X.; Song, J. H.; Song, D. K.; Yong, V. W.; Shuaib, A.; Hao, C. Cyclin-dependent kinase-5 prevents neuronal apoptosis through ERK-mediated upregulation of Bcl-2. *Cell Death Differ.* **2006**, *13*, 1203–1212.

(14) Dhavan, R.; Tsai, L. H. A decade of CDK5. *Nat. Rev. Mol. Cell Biol.* **2001**, *2*, 749–759.

(15) Ahn, J. S.; Radhakrishnan, M. L.; Mapelli, M.; Choi, S.; Tidor, B.; Cuny, G. D.; Musacchio, A.; Yeh, L. A.; Kosik, K. S. Defining Cdk5 ligand chemical space with small molecule inhibitors of tau phosphorylation. *Chem. Biol.* **2005**, *12*, 811–823.

(16) Clare, P. M.; Poorman, R. A.; Kelley, L. C.; Watenpaugh, K. D.; Bannow, C. A.; Leach, K. L. The cyclin-dependent kinases cdk2 and cdk5 act by a random, anticooperative kinetic mechanism. *J. Biol. Chem.* **2001**, *276*, 48292–49299.

(17) Kozakov, D.; Hall, D. R.; Beglov, D.; Brenke, R.; Comeau, S. R.; Shen, Y.; Li, K.; Zheng, J.; Vakili, P.; Paschalidis, I. C.; Vajda, S. Achieving reliability and high accuracy in automated protein docking: ClusPro, PIPER, SDU, and stability analysis in CAPRI rounds 13-19. *Proteins* **2010**, *78*, 3124–3130.

(18) Kozakov, D.; Brenke, R.; Comeau, S. R.; Vajda, S. PIPER: An FFT-based protein docking program with pairwise potentials. *Proteins* **2006**, *65*, 392–406.

(19) Kozakov, D.; Beglov, D.; Bohnuud, T.; Mottarella, S. E.; Xia, B.; Hall, D. R.; Vajda, S. How good is automated protein docking? *Proteins* **2013**, *81*, 2159–2166.

(20) Comeau, S. R.; Gatchell, D. W.; Vajda, S.; Camacho, C. J. ClusPro: A fully automated algorithm for protein-protein docking. *Nucleic Acids Res.* **2004**, *32*, W96–W99.

(21) Comeau, S. R.; Gatchell, D. W.; Vajda, S.; Camacho, C. J. ClusPro: An automated docking and discrimination method for the prediction of protein complexes. *Bioinformatics* **2003**, *20*, 45–50.

(22) Amato, A. A.; Rajagopalan, S.; Lin, J. Z.; Carvalho, B. M.; Figueira, A. C. M.; Lu, J.; Ayers, S. D.; Mottin, M.; Silveira, R. L.; Souza, P. C. T., et al. GQ-16, a novel peroxisome proliferator-activated receptor γ (PPARγ) ligand, promotes insulin sensitization without weight gain. *J. Biol. Chem.* **2012**, *287*, 28169–28179.

(23) Nolte, R. T.; Wisely, G. B.; Westin, S.; Cobb, J. E.; Lambert, M. H.; Kurokawa, R.; Rosenfeld, M. G.; Willson, T. M.; Glass, C. K.; Milburn, M. V. Ligand binding and co-activator assembly of the peroxisome proliferator-activated receptor-gamma. *Nature* **1998**, *395*, 137–143.

(24) Gampe Jr., R. T.; Montana, V. G.; Lambert, M. H.; Miller, A. B.; Bledsoe, R. K.; Milburn, M. V.; Kliewer, S. A.; Willson, T. M.; Xu, H. E. Asymmetry in the PPARgamma/RXRalpha crystal structure reveals the molecular basis of heterodimerization among nuclear receptors. *Mol. Cell* **2000**, *5*, 545–555.

(25) Berman, H. M.; Westbrook, J.; Feng, Z.; Gilliland, G.; Bhat, T. N.; Weissig, H.; Shindyalov, I. N.; Bourne, P. E. The protein data bank. *Nucleic Acids Res.* **2000**, *28*, 235–242.

(26) Bao, Z. Q.; Jacobsen, D. M.; Young, M. A. Briefly bound to activate: Transient binding of a second catalytic magnesium activates the structure and dynamics of CDK2 kinase for catalysis. *Structure* **2011**, *19*, 675–690.

(27) Gordon, J. C.; Myers, J. B.; Folta, T.; Shoja, V.; Heath, L. S.; Onufriev, A. H++: A server for estimating pKas and adding missing hydrogens to macromolecules. *Nucleic Acids Res.* **2005**, *33*, W368–W371.

(28) Humphrey, W.; Dalke, A.; Schulten, K. VMD - Visual molecular dynamics. *J. Molec. Graph.* **1996**, *14*, 33–38.

(29) Phillips, J. C.; Braun, R.; Wang, W.; Gumbart, J.; Tajkhorshid, E.; Villa, E.; Chipot, C.; Skeel, R. D.; Kalé, L.; Schulten, K. Scalable molecular dynamics with NAMD. *J. Comput. Chem.* **2005**, *26*, 1781–1802.

(30) Mackerell Jr., A. D.; Bashford, D.; Bellott, M.; Dunbrack Jr., R. L.; Evanseck, J. D.; Field, M. J.; Fischer, S.; Gao, J.; Guo, H.; Ha, S., et al. All-atom empirical potential for molecular modeling and dynamics studies of proteins. *J. Phys. Chem. B* **1998**, *102,* 3586–3616.

(31) Mackerell Jr., A. D.; Feig, M.; Brooks, C. L. Extending the treatment of backbone energetics in protein force fields: Limitations of gas-phase quantum mechanics in reproducing protein conformational distributions in molecular dynamics simulations. *J. Comput. Chem.* **2004**, *25*, 1400–1415.

(32) Jorgensen, W. L.; Chandrasekhar, J.; Madura, J. D.; Impey, R. W.; Klein, M. L. Comparison of simple potential functions for simulating liquid water. *J. Chem. Phys* **1983**, *79*, 926-935.

(33) Faller, C. E.; Reilly, K. A.; Hills, R. D.; Guvench, O. Peptide backbone sampling convergence with the adaptive biasing force algorithm. *J. Phys. Chem. B* **2013**, *117*, 518–26.

(34) Hénin, J.; Fiorin, G.; Chipot, C.; Klein, M. L. Exploring multidimensional free energy landscapes using time-dependent biases on collective variables. *J. Chem. Theory Comput.* **2010**, *6*, 35–47.

(35) Comer, J.; Gumbart, J. C.; Hénin, J.; Lelièvre, T.; Pohorille, A.; Chipot, C. The adaptive biasing force method: Everything you always wanted to know but were afraid to ask. *J. Phys. Chem. B* **2015**, *119*, 1129-1151.

(36) Leach, A. R. *Molecular Modelling: Principles and Applications;* Prentice Hall: New York, 2001; pp 334-352.

(37) Ryckaert, J.-P.; Ciccotti, G.; Berendsen, H. J. C. Numerical integration of the Cartesian equations of motion of a system with constraints: Molecular dynamics of n-alkanes. *J. Comput. Phys.* **1977**, *23*, 327–341.

(38) Laskowski, R. A.; MacArthur, M. W.; Moss, D. S.; Thornton, J. M. PROCHECK: A program to check the stereochemical quality of protein structures. *J. Appl. Cryst.* **1993**, *26*, 283–291.

(39) Laskowski, R. A.; Rullmann, J. A.; MacArthur, M. W.; Kaptein, R.; Thornton, J. M. AQUA and PROCHECK-NMR: Programs for checking the quality of protein structures solved by NMR. *J. Biomol. NMR* **1996**, *8*, 477–496.

(40) Mücksch, C.; Urbassek, H. M. Enhancing protein adsorption simulations by using accelerated molecular dynamics. *PLoS One* **2013**, *8*, e64883.

(41) Hamelberg, D.; Mongan, J.; McCammon, J. A. Accelerated molecular dynamics: A promising and efficient simulation method for biomolecules. *J. Chem. Phys.* **2004**, *120*, 11919–11929.

(42) Wang, Y.; Harrison, C. Implementation of accelerated molecular dynamics in NAMD. *Comput. Sci. Discov.* **2011**, *4*, 1–14.

(43) Wereszczynski, J.; McCammon, J. A. Accelerated molecular dynamics in computational drug design. In *Computational Drug Discovery and Design. Methods in Molecular Biology*; Baron R., Ed.; Humana Press: New York, 2012; pp 515-524.

(44) Chandra, V.; Huang, P.; Hamuro, Y.; Raghuram, S.; Wang, Y.; Burris, T. P.; Rastinejad, F. Structure of the intact PPAR-γ-RXR-α nuclear receptor complex on DNA. *Nature* **2008**, *456*, 350–356.

(45) Xu, Y.; Colletier, J. P.; Jiang, H.; Silman, I.; Sussman, J. L.; Weik, M. Induced-fit or preexisting equilibrium dynamics? Lessons from protein crystallography and MD simulations on acetylcholinesterase and implications for structure-based drug design. *Protein Sci.* **2008**, *17*, 601–605.

(46) Koshland, D. E. Application of a theory of enzyme specificity to protein synthesis. *Proc. Natl. Acad. Sci. U. S. A.* **1958**, *44*, 98–104.

(47) Tsai, C. J.; Kumar, S.; Ma, B.; Nussinov, R. Folding funnels, binding funnels, and protein function. *Protein Sci.* **1999**, *8*, 1181–1190.

(48) Monod, J.; Wyman, J.; Changeux, J. P. On the nature of allosteric transitions: A plausible model. *J. Mol. Biol.* **1965**, *12*, 88–118.

(49) Ubersax, J. A.; Ferrell, J. E. Mechanisms of specificity in protein phosphorylation. *Nat. Rev. Mol. Cell Biol.* **2007**, *8*, 530–541.

(50) Adams, P. D.; Sellers, W. R.; Sharma, S. K.; Wu, A. D.; Nalin, C. M.; Kaelin, W. G. J. Identification of a cyclin-cdk2 recognition motif present in substrates and p21-like cyclin-dependent kinase inhibitors. *Mol Cell Biol.* **1996**, *16*, 6623–6633.

(51) Schulman, B. A.; Lindstrom, D. L.; Harlow, E. Substrate recruitment to cyclin-dependent kinase 2 by a multipurpose docking site on cyclin A. *Proc. Natl. Acad. Sci. U.S.A.* **1998**, *95*, 10453–10458.

(52) Cheng, K. Y.; Noble, M. E.; Skamnaki, V.; Brown, N. R.; Lowe, E. D.; Kontogiannis, L.; Shen, K.; Cole, P.A.; Siligardi, G.; Johnson, L. N. The role of the phospho-CDK2/cyclin A recruitment site in substrate recognition. *J. Biol. Chem.* **2006**, *281*, 23167–23179.

(53) Stevenson-Lindert, L. M.; Fowler, P.; Lew, J. Substrate specificity of CDK2-cyclin A: What is optimal? *J. Biol. Chem.* **2003**, *278*, 50956–50960.

(54) Bruning, J. B.; Chalmers, M. J.; Prasad, S.; Busby, S. A.; Kamenecka, T. M.; He, Y.; Nettles, K. W.; Griffin, P. R. Partial agonists activate PPARgamma using a helix 12 independent mechanism. *Structure* **2007**, *15*, 1258–1271.

(55) Waku, T.; Shiraki, T.; Oyama, T.; Fujimoto, Y.; Maebara, K.; Kamiya, N.; Jingami, H.; Morikawa, K. Structural insight into PPARgamma activation through covalent modification with endogenous fatty acids. *J. Mol. Biol.* **2009**, *385*, 188–199.

(56) Bernardes, A.; Souza, P. C. T.; Muniz, J. R. C.; Ricci, C. G.; Ayers, S. D.; Parekh, N. M.; Godoy, A. S.; Trivella, D. B.; Reinach, P.; Webb, P.; Skaf, M. S., et al. Molecular mechanism of

peroxisome proliferator-activated receptor α activation by WY14643 : A new mode of ligand recognition and receptor stabilization. *J. Mol. Biol.* **2013**, *425*, 2878–2893.

(57) Martínez, L.; Sonoda, M. T.; Webb, P.; Baxter, J. D.; Skaf, M. S.; Polikarpov, I. Molecular dynamics simulations reveal multiple pathways of ligand dissociation from thyroid hormone receptors. *Biophys. J.* **2005**, *89*, 2011–2023.

(58) Martínez, L.; Polikarpov, I.; Skaf, M. S. Only subtle protein conformational adaptations are required for ligand binding to thyroid hormone receptors: Simulations using a novel multipoint steered molecular dynamics approach. *J. Phys. Chem. B* **2008**, *112*, 10741–10751.

(59) Martínez, L.; Webb, P.; Polikarpov, I.; Skaf, M. S. Molecular dynamics simulations of ligand dissociation from thyroid hormone receptors: Evidence of the likeliest escape pathway and its implications for the design of novel ligands. *J. Med. Chem.* **2006**, *49*, 23–26.

(60) Mahindroo, N.; Huang, C.F.; Peng, Y. H.; Wang, C. C.; Liao, C. C.; Lien, T. W.; Chittimalla, S. K.; Huang, W. J.; Chai, C. H.; Prakash, E., et al. Novel indole-based peroxisome proliferator-activated receptor agonists: Design, SAR, structural biology, and biological activities. *J. Med. Chem.* **2005**, *48*, 8194–8208.

(61) Mahindroo, N.; Wang, C. C.; Liao, C. C.; Huang, C. F.; Lu, I. L.; Lien, T. W.; Peng, Y. H.; Huang, W. J.; Lin, Y. T.; Hsu, M. C., et al. Indol-1-yl acetic acids as peroxisome proliferator-activated receptor agonists: Design, synthesis, structural biology, and molecular docking studies. *J. Med. Chem.* **2006**, *49*, 1212–1216.

(62) Pochetti, G.; Godio, C.; Mitro, N.; Caruso, D.; Galmozzi, A.; Scurati, S.; Loiodice, F.; Fracchiolla, G.; Tortorella, P.; Laghezza, A., et al. Insights into the mechanism of partial agonism: Crystal structures of the peroxisome proliferator-activated receptor gamma ligand-binding domain in the complex with two enantiomeric ligands. *J. Biol. Chem.* **2007**, *282*, 17314–17324.

(63) Montanari, R.; Saccoccia, F.; Scotti, E.; Crestani, M.; Godio, C.; Gilardi, F.; Loiodice, F.; Fracchiolla, G.; Laghezza, A.; Tortorella, P., et al. Crystal structure of the peroxisome proliferator-activated receptor gamma (PPARgamma) ligand binding domain complexed with a novel partial agonist: A new region of the hydrophobic pocket could be exploited for drug design. *J. Med. Chem.* **2008**, *51*, 7768–7776.

(64) Hughes, T. S.; Giri, P. K.; de Vera, I. M. S.; Marciano, D. P.; Kuruvilla, D. S.; Shin, Y.; Blayo, A.; Kamenecka, T. M.; Burris, T. P.; Griffin, P. R., et al. An alternate binding site for PPARγ ligands. *Nat. Commun.* **2014**, *5*, 1–28.

(65) Leitner, A.; Walzthoeni, T.; Kahraman, A.; Herzog, F.; Rinner, O.; Beck, M.; Aebersold, R. Probing native protein structures by chemical cross-linking, mass spectrometry, and bioinformatics. *Mol. Cell. Proteomics* **2010**, *9*, 1634–1649.

(66) Walzthoeni, T.; Leitner, A.; Stengel, F.; Aebersold, R. Mass spectrometry supported determination of protein complex structure. *Curr. Opin. Struct. Biol.* **2013**, *23*, 252–260.

FIGURE CAPTIONS

Figure 1. Modeling strategy for the PPARγ-Cdk5/p25: **A)** Initial crystallographic/modeling structures of Cdk5/p25 and PPARγ; **B)** Protein-protein docking and selection based on the biochemistry of phosphorylation and the full length PPARγ-RXRα crystallographic structure; **C)** Refinement of the models via ABF MD simulations in order to achieve molecular configuration at the catalytic site adequate for the reaction; **D)** Validation of the PPARγ-Cdk5/p25 models stability via MD simulations.

Figure 2. A) Schematic ABF simulations: Starting from selected protein-protein docked poses, further structural adjustments are obtained using ABF MD simulations that use an available Cdk2/p25-peptide crystal structure as target. The refined model was further validated by means of MD simulations. **B)** Superimposed structures at the catalytic site from target (Cdk2-peptide) and Cdk5-S245 loop after ABF runs; **C)** Time history of selected molecular separations and RMSD values during the course oft the ABF MD runs.

Figure 3. Structural features of the PPARγ-Cdk5/p25 models before (gray) and after (color) ABF MD refinement: **A)** Structures aligned by PPARγ for Model 1 (orange), Model 2 (blue), Model 3 (magenta) and Model 4 (green). Cdk5/p25 is shown in violet; **B)** Average RMSD taken from the last 10 ns of ABF simulation computed for backbone atoms and crystallographic structure as reference.

Figure 4. Local changes in the active site during refinement: **A)** Average RMSD of S245 loop – β-strand backbone region of the complexed PPARγ (10 ns last ABF MD) and the free-PPARγ (entire 200 ns aMD runs), using the PPARγ crystallographic structure (PDB ID: 3T03) as reference; **B)** percentage of contacts (relative to the PPARγ crystallographic structure (PDB ID: 3T03) between S245 loop and

LBD core; **C)** Superimposed S245 loop – β-strand structures from aMD simulations (gray) and snapshots taken from the ABF MD models (1, orange; 2, blue; 3, magenta; 4, green). The crystallographic structure (PDB ID: 3T03) is shown for comparison (dark gray).

Figure 5. A) Distance between the phosphorylation residues, the hydroxyl H of S245 (PPARγ) and oxygen atom of D126 (Cdk5) during MD runs for PPARγ-Cdk5/p25 Model 1 (orange), Model 2 (blue), Model 3 (magenta), and Model 4 (green). The S245 residue departs from D126 in Models 1, 2 and, in Model 4, Cdk5 and PPARγ completely dissociate. Panels B), C), D) and E) show the active site of PPARγ-Cdk5/p25 models after 300 ns of MD simulations.

Figure 6. Structural characterization of PPARγ-Cdk5/p25 Model 3: (**A**) The three docking regions between PPARγ (magenta) and Cdk5 (violet) and p25 (white): Ω-loop site (transparent red surface), active site (transparent green) and β-sheet site (transparent yellow surface). PPARγ and Cdk5/p25 interactive residues (H-bonds represented by dotted line and hydrophobic interaction by the transparent surface): in Ω-loop site (**B**); in active site (**C**); in β-sheet site (**D**). Number of hydrophilic and hydrophobic contacts in each site (**E**).

Figure 7. A) Aligned crystallographic holo-PPARγ structures (2ATH.pdb, 2F4B.pdb, 2I4Z.pdb, 3B3K.pdb) showing the Ω-loop region (red) close to the LBD core; **B)** PPARγ-Cdk5/p25 Model 3 showing the Ω-loop (red) in an open configuration.

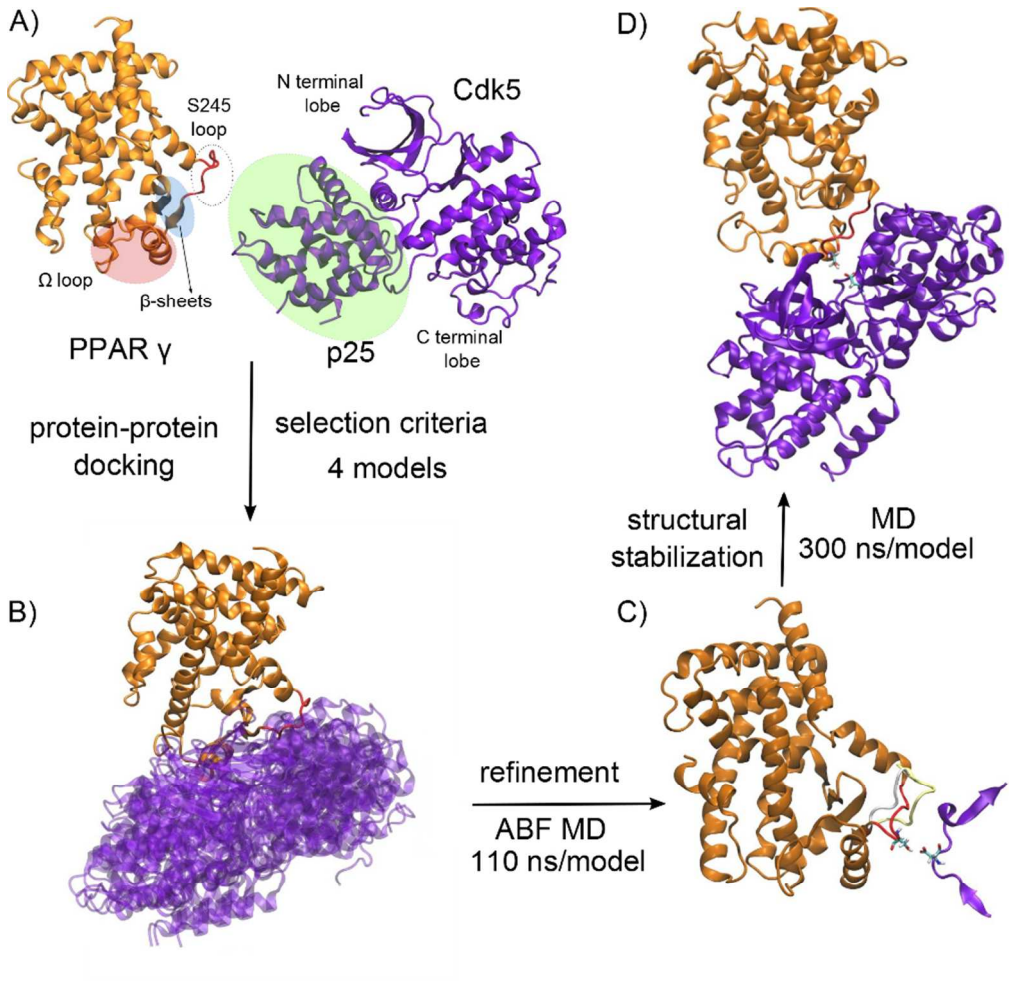

Figure 1
84x82mm (300 x 300 DPI)

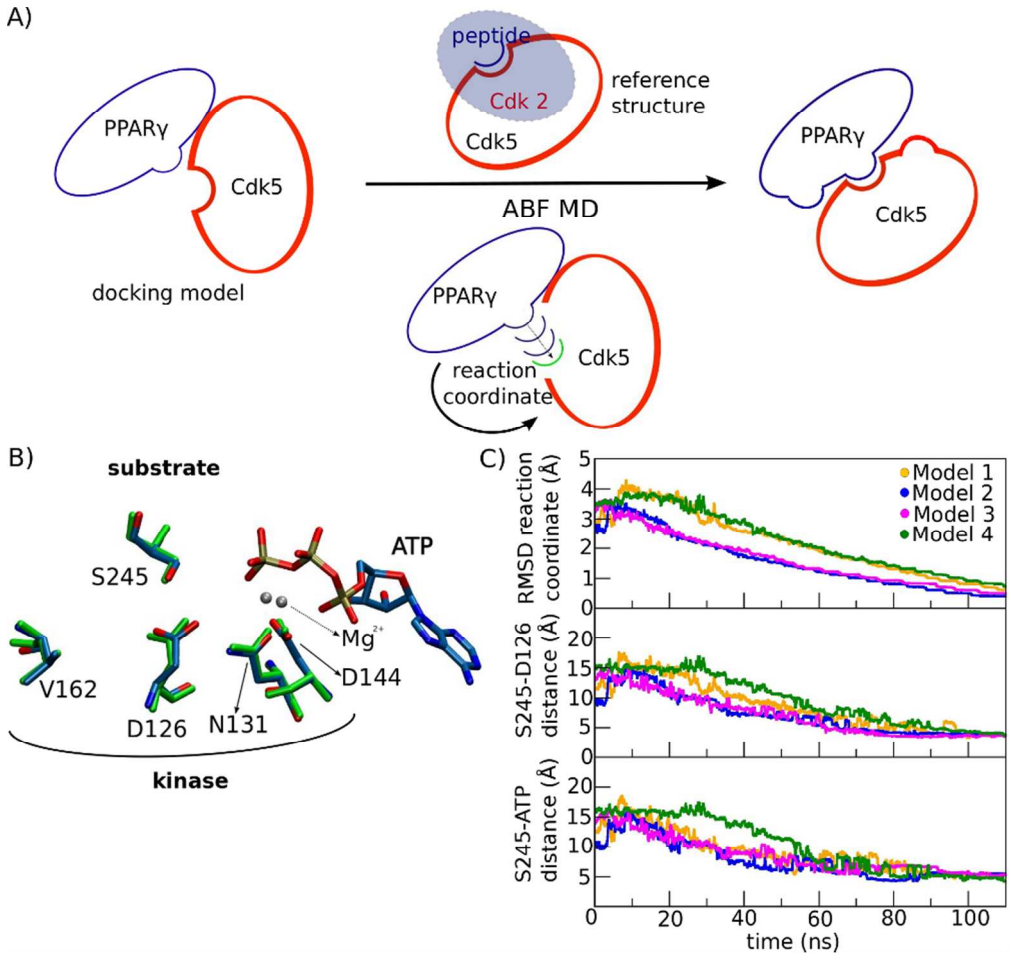

Figure 2
84x79mm (300 x 300 DPI)

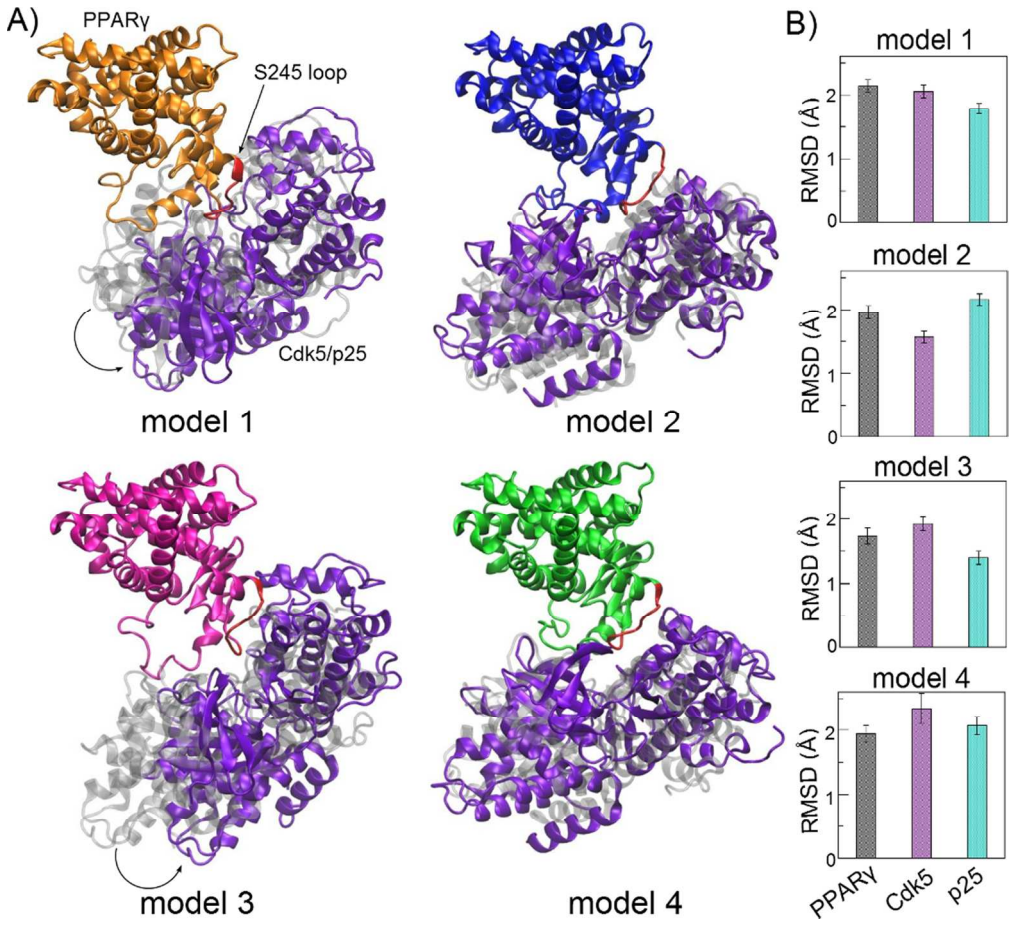

Figure 3
92x84mm (300 x 300 DPI)

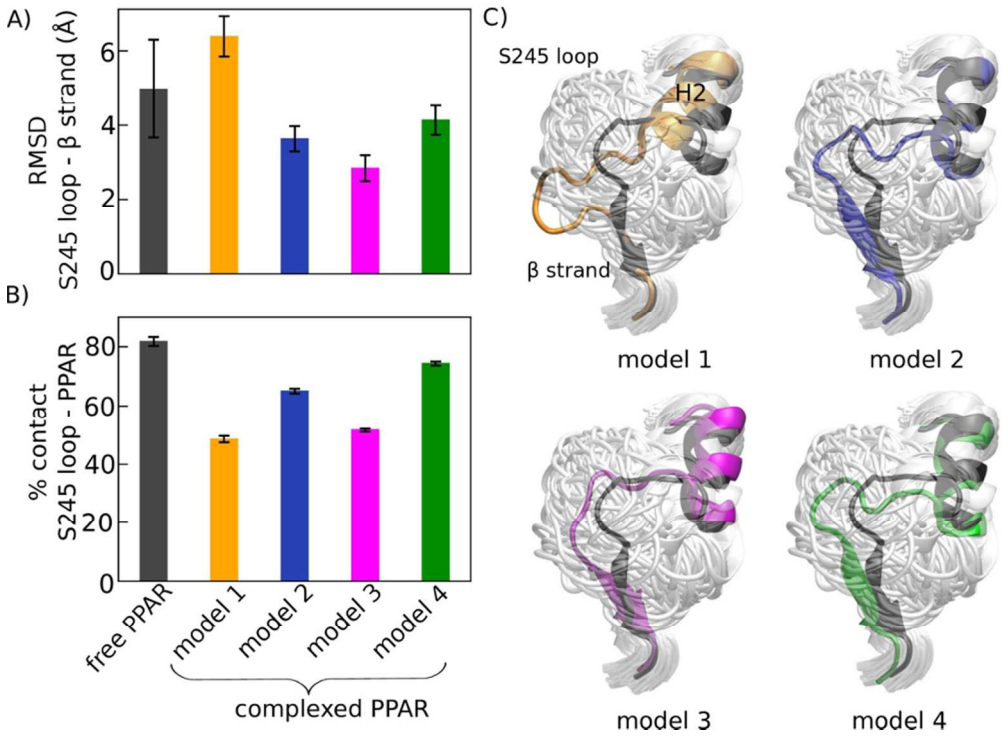

Figure 4
84x61mm (300 x 300 DPI)

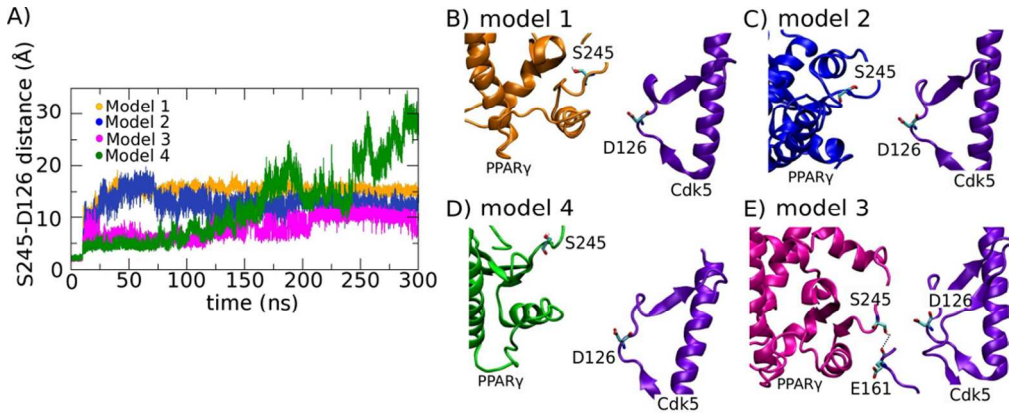

Figure 5
101x41mm (300 x 300 DPI)

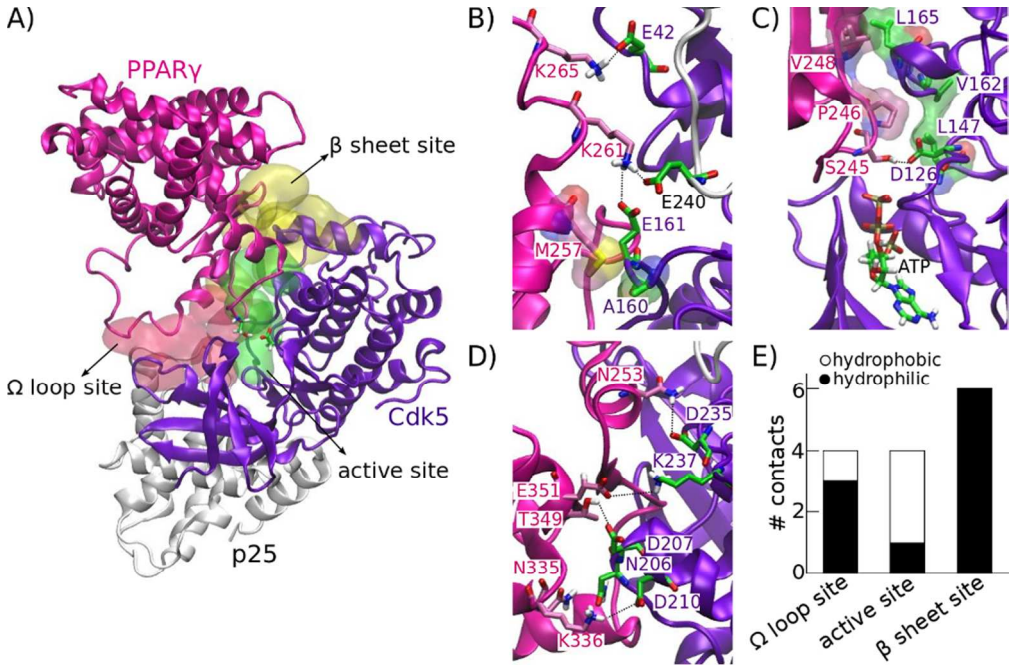

Figure 6
84x55mm (300 x 300 DPI)

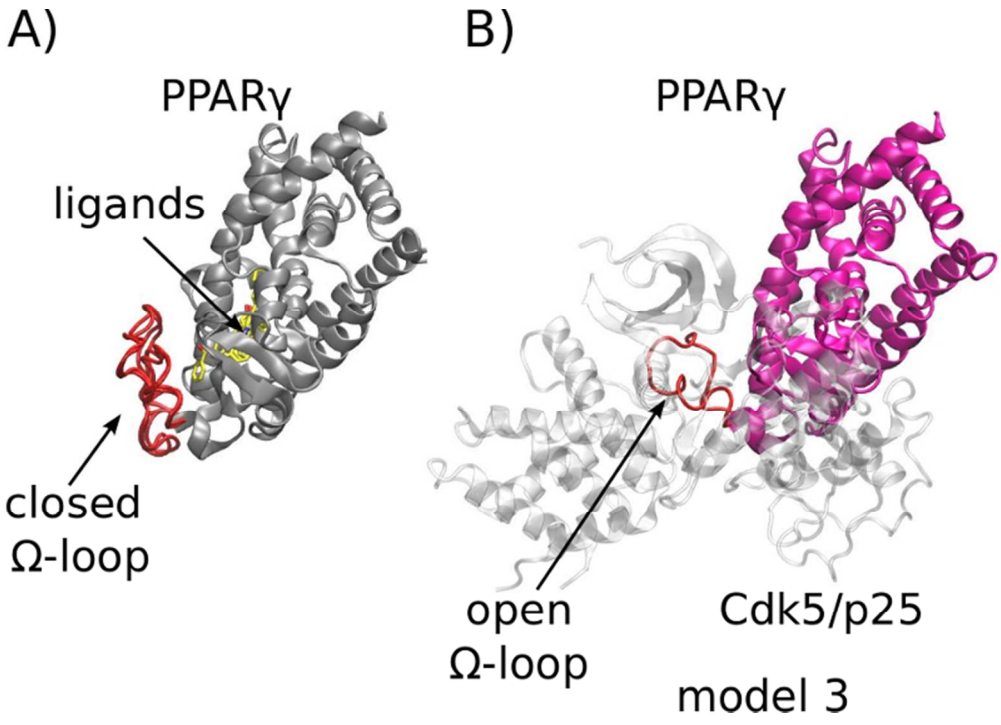

Figure 7
67x47mm (300 x 300 DPI)

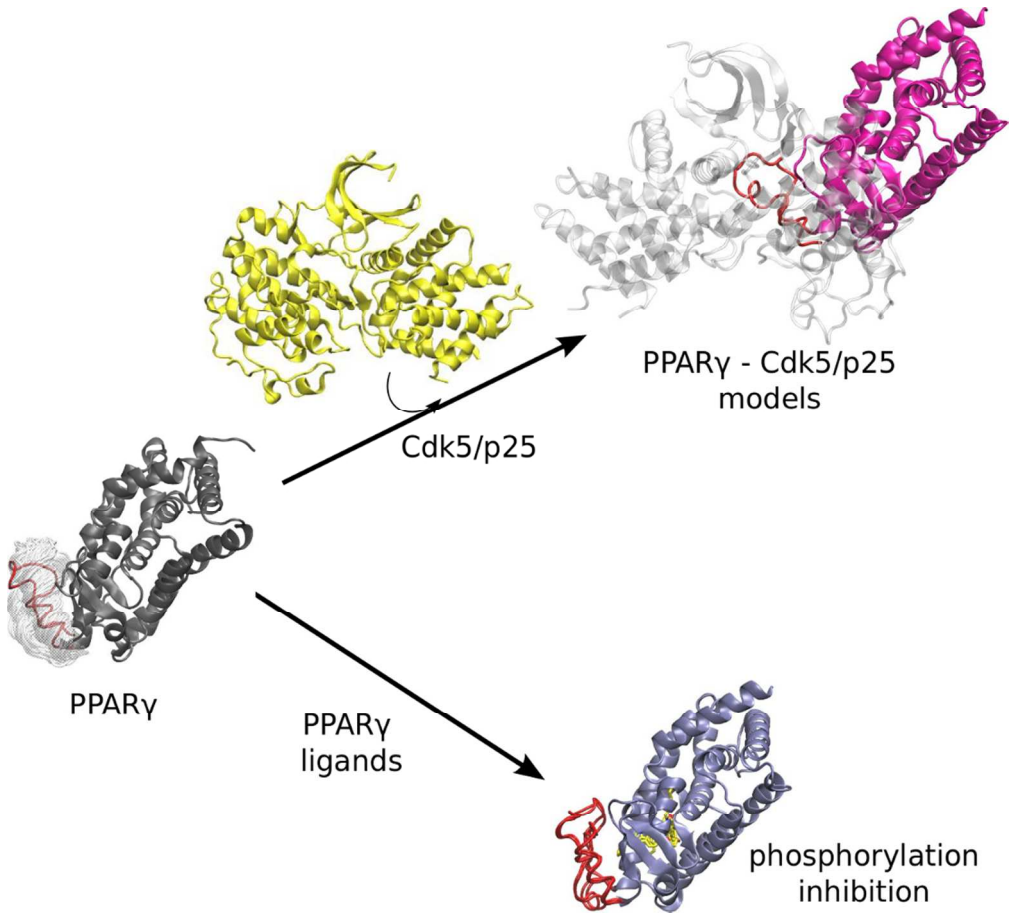

TOC Graphics
93x84mm (300 x 300 DPI)